JOURNAL OF AIRCRAFT
Vol. 45, No. 5, September–October 2008

A z-Transform Discrete-Time State-Space Formulation for Aeroelastic Stability Analysis

Alexandre Noll Marques*
Instituto Tecnologico de Aeronáutica, 12228-900 São José dos Campos, Brazil
and
João Luiz F. Azevedo†
Instituto de Aeronáutica e Espaco, 12228-903 São José dos Campos, Brazil

DOI: 10.2514/1.32561

In many complex aerospace applications, it is common to use numerical tools to evaluate the unsteady aerodynamic behavior. The present work presents an alternate formulation for the state-space representation of aeroelastic systems based on digital control theory that is shown to be more effective and accurate for the coupling of numerical solutions with such systems. The application of the z transform allows for direct frequency domain representations of the aerodynamic solutions without the need for approximating models, as generally occurs in other state-space formulations. This fact also makes this new methodology a more straightforward procedure for aeroelastic analyses. A typical section model of a NACA 0012 airfoil at transonic flow conditions is used as a test case to assess the correctness and accuracy of the proposed formulation. The present results are compared with data obtained from continuous-time state-space formulations and through the direct integration of the aerodynamic and structural dynamic equations.

Introduction

THE lack of accurate aerodynamic analytical models for complex flow situations makes the solution of realistic aeroelastic problems a very difficult task. Over the years, approximate solutions of the aerodynamic potential theory [1–3] and, more recently, numerical solutions obtained with computational fluid dynamics (CFD) solvers [4–11] have been used to represent the aerodynamic response to generic structural behavior to decouple the aerodynamic and structural effects. Such aerodynamic data are generally modeled with rational functions [12] or interpolating polynomials [13–15] in a convenient fashion so as to represent the aeroelastic system through a state-space formulation. Some of the most common state-space formulations used nowadays for aeroelastic stability analyses are described in the following sections.

There are also recent approaches [16–18] that directly result in time domain state-space representations of the aeroelastic system. Such approaches, which are not described in further detail in this paper, use eigensystem realization algorithms (ERAs) to identify the state-space representation from the aerodynamic impulsive responses. Furthermore, there is also work in the literature which is concerned with applying a single-composite input (SCI) to obtain the system aerodynamic impulse responses and, hence, minimize the time and cost for the construction of the aeroelastic model [18]. Such approaches are also beyond the scope of the present paper.

The present work presents an alternate approach for the state-space representation of aeroelastic systems based on discrete-time control techniques. The main idea behind this approach is to avoid the need for an approximate model of the aerodynamic responses. This goal is achieved by calculating the aerodynamic characteristics in the frequency domain with the direct use of the z transform. The complete formulation of the new state-space representation is also presented. Finally, a typical section model of a NACA 0012 airfoil at transonic flow conditions is used as a test case for a detailed comparison of the different state-space formulations and direct integration results.

The CFD solver employed for evaluating the aerodynamic responses contained in the present work is the same as that presented in [11,19,20]. It is based on the 2-D Euler equations, which represent two-dimensional, compressible, rotational, inviscid, and nonlinear flows. Therefore, it is completely capable of capturing the shock waves present in transonic flows. These equations are discretized in space with a cell centered, finite volume scheme, and they are advanced in time using a second-order accurate, five-stage, explicit, hybrid Runge–Kutta scheme. It is clear that the determination of impulsive aerodynamic responses is an important part of the overall aeroelastic stability analysis procedure proposed here. The present paper, however, will not address this issue. The interested reader is referred to [20] for further details on how such responses are calculated in the present case. Moreover, as far as the present aeroelastic stability analysis procedure is concerned, provided that a set of discrete-time aerodynamic responses is available, the methodology can be applied regardless of how such aerodynamic data were obtained. In the present work, the aerodynamic responses are obtained using CFD simulations.

Theoretical Formulation

A general aeroelastic system is characterized by aerodynamic, elastic, and inertial forces dynamically interacting with structural deformations. It is very common, therefore, to represent the aerodynamic effects exclusively through the resulting forces and moments acting on the structure as a forcing term. The methodology proposed in the present work is focused on the adequate representation of the aerodynamic operator for complex flow situations. Hence, it is instructive to apply such methodology over simple structural models to avoid further complications that might hide the behavior of the aerodynamic model. The structural model considered in the present work is the typical section, which is widely known and reported in the literature [2,9]. The dynamic system represented in the typical section is a rigid airfoil with 2 deg of freedom, plunge, and pitch, as shown in Fig. 1. As presented in Fig. 1, α is the pitch mode coordinate, positive in the nose-up direction, and h is the vertical translation, positive downward. Moreover, c is the

Presented as Paper 3800 at the 25th AIAA Applied Aerodynamics Conference, Miami, FL, 25–28 June 2007; received 1 June 2007; revision received 10 February 2008; accepted for publication 19 February 2008.

*M.S. Student, Division of Aeronautical Engineering, Comando-Geral de Tecnologia Aeroespacial; ale_noll@yahoo.com. Student Member AIAA.

†Senior Research Engineer, Aerodynamics Division, Comando-Geral de Tecnologia Aeroespacial; azevedo@iae.cta.br. Associate Fellow AIAA.

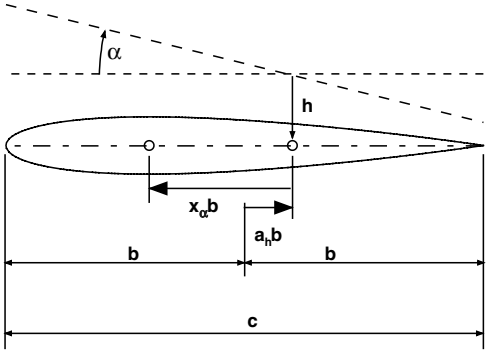

Fig. 1 Typical section configuration.

airfoil chord length, whereas b is its semichord length. Finally, x_α is the distance from the elastic axis to the center of mass and a_h is the distance from midchord to the elastic axis, both nondimensionalized using the semichord length (b).

The governing equation for the motion of such a dynamic system is given by

$$[M]\{\ddot{\eta}(t)\} + [K]\{\eta(t)\} = \{Qa(t)\} \tag{1}$$

where the generalized mass and stiffness matrices are, respectively,

$$[M] = \begin{bmatrix} 1 & x_\alpha \\ x_\alpha & r_\alpha^2 \end{bmatrix} \quad \text{and} \quad [K] = \begin{bmatrix} \omega_h^2 & 0 \\ 0 & r_\alpha^2\omega_\alpha^2 \end{bmatrix} \tag{2}$$

and the generalized coordinate and force vectors are

$$\{\eta(t)\} = \begin{Bmatrix} \xi(t) \\ \alpha(t) \end{Bmatrix} \quad \text{and} \quad \{Qa(t)\} = \begin{Bmatrix} \frac{Qa_h(t)}{mb} \\ \frac{Qa_\alpha(t)}{mb^2} \end{Bmatrix} \tag{3}$$

In Eq. (2), r_α denotes the airfoil dimensionless radius of gyration about the elastic axis, m is the airfoil mass, and ω_h and ω_α are the uncoupled natural circular frequencies of the plunge and pitch modes, respectively. Furthermore, in Eq. (3), ξ is the plunge mode coordinate, where $\xi = h/b$.

It is convenient to nondimensionalize the aeroelastic equation to represent more general situations. This is accomplished with the procedure proposed by Oliveira [9], using a reference circular frequency to nondimensionalize the time variable:

$$\bar{t} = t\omega_r \tag{4}$$

With the application of the chain rule for the time derivatives,

$$\frac{\mathrm{d}(\cdot)}{\mathrm{d}t} = \frac{\mathrm{d}(\cdot)}{\mathrm{d}\bar{t}}\frac{\mathrm{d}\bar{t}}{\mathrm{d}t} = \omega_r\frac{\mathrm{d}(\cdot)}{\mathrm{d}\bar{t}} \tag{5}$$

Eq. (1) becomes

$$[M]\{\ddot{\eta}(\bar{t})\} + [\bar{K}]\{\eta(\bar{t})\} = \{\bar{Q}a(\bar{t})\} \tag{6}$$

where

$$[\bar{K}] = \left(1/\omega_r^2\right)[K] \quad \text{and} \quad \{\bar{Q}a(\bar{t})\} = \left(1/\omega_r^2\right)\{Qa(\bar{t})\} \tag{7}$$

As previously mentioned, the main objective of the present study is to efficiently determine the generalized aerodynamic force vector, $\{\bar{Q}a(\bar{t})\}$, for an arbitrary structural behavior. However, due to the nonlinearities of the aerodynamic equations, it is very difficult to obtain a general expression for the aerodynamic response. However, this problem is simplified by extending linearity concepts present in the formulation of the potential aerodynamic equations. As presented in [2,12], the linear aerodynamic responses can be individually determined for each mode and then superimposed for more general responses. Based on these ideas, Oliveira [9] proposed the assumption of linearity of the aerodynamic response in the transonic regime with regard to the modal motion. As there are no rigorous linearization procedures involved, there are no guarantees that such an assumption holds. But, it is natural to expect this sort of linear hypothesis to be valid at least for small amplitudes. Actually, as shown later in this paper, there is a certain amplitude range in which this hypothesis holds.

Furthermore, it is important to emphasize that the aeroelastic phenomena analyzed in the present work are restricted to small amplitude motions. Therefore, when considering flutter, which is characterized by diverging oscillations, only the onset of this phenomenon can be identified with such an approach. There may occur situations in which the aerodynamic nonlinear behavior suppresses the diverging oscillations creating limit cycle oscillations, and the present formulation may not correctly capture such cases. Nevertheless, for safety reasons, most designers are interested in the flutter onset point.

As a consequence of the linearity assumptions, it is possible to determine the aerodynamic response to a general structural behavior from the convolution of an impulsive or indicial aerodynamic solution [2,19–21]. The convolution operation, however, is more easily handled in the frequency domain, in which it is represented by a simple multiplication operation. Hence, the aerodynamic forces linearized with regard to the modal displacements can be written, in the frequency domain, as

$$L(\kappa) = L_{I_h}(\kappa)h(\kappa) + L_{I_\alpha}(\kappa)\alpha(\kappa) \tag{8}$$

$$M_y(\kappa) = M_{I_h}(\kappa)h(\kappa) + M_{I_\alpha}(\kappa)\alpha(\kappa) \tag{9}$$

In Eqs. (8) and (9), the reduced frequency κ is used to represent the frequency domain. Moreover, L designates the lift force, and M_y the pitching moment with respect to the elastic axis, positive in the nose-up direction. The $h(\kappa)$ and $\alpha(\kappa)$ variables represent the amplitudes of the frequency content of motions in plunge and pitch modes, respectively, whereas the $L_{I_h}(\kappa)$, $L_{I_\alpha}(\kappa)$, $M_{I_h}(\kappa)$, and $M_{I_\alpha}(\kappa)$ coefficients indicate complex numbers that designate the magnitude and phase delay of the generalized forces with respect to unitary-amplitude harmonic motions of the respective structural mode. If one considers the usual definitions of aerodynamics, it follows that the lift and moment coefficients are given, respectively, by

$$C_\ell(\kappa) = \frac{L(\kappa)}{\frac{1}{2}\rho_\infty U_\infty^2 c} = \frac{L_{I_h}(\kappa)h(\kappa)}{\frac{1}{2}\rho_\infty U_\infty^2 c} + \frac{L_{I_\alpha}(\kappa)\alpha(\kappa)}{\frac{1}{2}\rho_\infty U_\infty^2 c} \tag{10}$$

$$C_m(\kappa) = \frac{M_y(\kappa)}{\frac{1}{2}\rho_\infty U_\infty^2 c^2} = \frac{M_{I_h}(\kappa)h(\kappa)}{\frac{1}{2}\rho_\infty U_\infty^2 c^2} + \frac{M_{I_\alpha}(\kappa)\alpha(\kappa)}{\frac{1}{2}\rho_\infty U_\infty^2 c^2} \tag{11}$$

Following the generalized coordinate notation of Eqs. (3) and (7), the generalized forces are finally given by

$$\bar{Q}a_h(\kappa) = -\frac{L(\kappa)}{mb\omega_r^2} = -\frac{\rho_\infty U_\infty^2}{m\omega_r^2}\left[C_{\ell_{Ih}}(\kappa)\frac{\xi(\kappa)}{2} + C_{\ell_{I\alpha}}(\kappa)\alpha(\kappa)\right] \tag{12}$$

$$\bar{Q}a_\alpha(\kappa) = \frac{M_y(\kappa)}{mb^2\omega_r^2} = \frac{\rho_\infty U_\infty^2}{m\omega_r^2}[C_{m_{Ih}}(\kappa)\xi(\kappa) + 2C_{m_{I\alpha}}(\kappa)\alpha(\kappa)] \tag{13}$$

or

$$\{\bar{Q}a(\kappa)\} = \frac{(U^*)^2}{\pi\mu}[A(\kappa)]\{\eta(\kappa)\} \tag{14}$$

where the mass ratio is defined as

$$\mu = m/\pi\rho_\infty b^2 \tag{15}$$

the characteristic speed is

$$U^* = U_\infty/b\omega_r \tag{16}$$

and the aerodynamic influence coefficient matrix is given by

$$[A(\kappa)] = \begin{bmatrix} -C_{\ell_{Ih}}(\kappa)/2 & -C_{\ell_{I\alpha}}(\kappa) \\ C_{m_{Ih}}(\kappa) & 2C_{m_{I\alpha}}(\kappa) \end{bmatrix} \tag{17}$$

Moreover, ρ_∞ and U_∞ designate, respectively, the undisturbed flow density and speed.

There are different approaches that can be used to determine the desired aerodynamic coefficients. As there is no closed-form solution for the compressible subsonic and transonic unsteady aerodynamic forces, this work is aimed at numerical methods in which the impulsive solution is known for a determined number of discrete reduced frequency values. However, the calculation of aerodynamic responses in the frequency domain is beyond the scope of the present paper, and it is assumed that this information is known a priori.

Just to name a few possibilities for the calculation of such responses, for the compressible subsonic regime, there are numerical methods for the solution of integral equations, tabulated results [1,3], and approximate formulas [22] for the linearized potential equations [2]. More realistic solutions, especially for the transonic regime, can be achieved with modern CFD solvers, either with the solution of harmonic oscillations [5,7] or by the direct and indirect determination of impulsive or indicial responses [4,6,8,10,11]. All the aerodynamic responses presented here are obtained by exciting the aerodynamic system in a frequency range of interest through the individual application of a smooth pulse motion in both modes [11,19,20].

Continuous-Time State-Space Formulation

General Formulation

A state-space representation of a system corresponds to the description of the system dynamics in terms of first-order differential equations, which may be combined into a first-order vector–matrix differential equation [23]. In the present case, this formulation can be achieved by defining [9]

$$\{x_1(\bar{t})\} = \{\eta(\bar{t})\} \tag{18}$$

$$\{x_2(\bar{t})\} = \{\dot{\eta}(\bar{t})\} = \{\dot{x}_1(\bar{t})\} \tag{19}$$

$$\{x(\bar{t})\} = \begin{Bmatrix} \{x_2(\bar{t})\} \\ \{x_1(\bar{t})\} \end{Bmatrix} \tag{20}$$

where $\{x(\bar{t})\}$ is the system state vector. Hence, the governing equation of motion becomes

$$[\tilde{M}]\{\dot{x}(\bar{t})\} + [\tilde{K}]\{x(\bar{t})\} = \{\tilde{q}(\bar{t})\} \tag{21}$$

where

$$[\tilde{M}] = \begin{bmatrix} [M] & [0_{2\times2}] \\ [0_{2\times2}] & [I_{2\times2}] \end{bmatrix}, \qquad [\tilde{K}] = \begin{bmatrix} [0_{2\times2}] & [\bar{K}] \\ -[I_{2\times2}] & [0_{2\times2}] \end{bmatrix} \tag{22}$$

and

$$\{\tilde{q}(\bar{t})\} = \begin{Bmatrix} \{\bar{Q}a(\bar{t})\} \\ \{0_{2\times1}\} \end{Bmatrix} \tag{23}$$

If one considers that the aerodynamic forces can be conveniently represented in the frequency domain, the system can be more easily studied in the Laplace domain. Applying the Laplace transform to Eq. (21), one obtains

$$\bar{s}[\tilde{M}]\{X(\bar{s})\} + [\tilde{K}]\{X(\bar{s})\} = \{\tilde{Q}(\bar{s})\} \tag{24}$$

where

$$\bar{s} = s/\omega_r \tag{25}$$

is the dimensionless Laplace transform complex variable. The idea behind this procedure is to evaluate the aerodynamic influence coefficient matrix over a reduced frequency range of interest and, by making use of the analytical continuation principle [24], to extend such a result to the entire complex plane.

As previously discussed, the available aerodynamic responses in the frequency domain consist of sets of numerical values, which are not convenient for the solution of Eq. (24). Therefore, it is necessary to approximate these data using interpolating polynomials. There are a number of different polynomials reported in the literature [12,13,25,26], from which the ones suggested by Roger [13] and Eversman and Tewari [25,26] were selected by the authors for implementation and tests. This choice is based on the fact that such polynomials are the most commonly used in applications similar to the ones intended in the present work and that they are conveniently constructed for the formulation of aerodynamic state variables. Moreover, although these polynomials are very similar, they result in different aerodynamic state variables. Hence, the state-space problem is slightly different for each of the polynomials used. The adopted approximating polynomials and the resulting state-space formulations are all presented in the following subsections.

Regardless of which polynomial is used for the representation of the aerodynamic response in the Laplace domain, the resulting state-space representation of the typical section aeroelastic system has always the form

$$\{\dot{\chi}(\bar{t})\} = [D]\{\chi(\bar{t})\} \tag{26}$$

$\{\chi(\bar{t})\}$ is the new state vector that results from the addition of the aerodynamic state variables,

$$\{\chi(\bar{t})\} = \begin{Bmatrix} \{\dot{\eta}(\bar{t})\} \\ \{\eta(\bar{t})\} \\ \{\eta_a(\bar{t})\}_1 \\ \vdots \\ \{\eta_a(\bar{t})\}_{n_a} \end{Bmatrix} \tag{27}$$

where n_a is the number of added aerodynamic state variables. Moreover, $[D]$ is the stability matrix of the system, which can be written as

$$[D] = \begin{bmatrix} [D_{\eta\eta}] & [D_{\eta a}] \\ [D_{a\eta}] & [D_{aa}] \end{bmatrix} \tag{28}$$

where

$$[D_{\eta\eta}] = \begin{bmatrix} -[\mathcal{M}]^{-1}[\mathcal{C}] & -[\mathcal{M}]^{-1}[\mathcal{K}] \\ [I_{2\times2}] & [0_{2\times2}] \end{bmatrix} \tag{29}$$

$$[\mathcal{M}] = [M] - (1/\pi\mu)[A_2] \tag{30}$$

$$[\mathcal{K}] = [\bar{K}] - ((U^*)^2/\pi\mu)[A_0] \tag{31}$$

$$[\mathcal{C}] = -(U^*/\pi\mu)[A_1] \tag{32}$$

and the $[A_n]$ matrices come from the interpolating polynomial representations of the aerodynamic forces, as presented next. The other terms of the stability matrix also depend on the choice of the interpolating polynomial. Finally, the aeroelastic stability analysis can then be reduced to the classical eigenvalue problem for each value of the U^* parameter,

$$([D] - \bar{s}[I_{N\times N}])\{\chi(\bar{s})\} = \{0_{N\times1}\} \tag{33}$$

where $N = 2n_a + 4$.

Roger Polynomial

The polynomial proposed by Roger [13] is the same used by Oliveira [9] and Abel [14]. It is given, already in the Laplace domain, by

$$[A(\bar{s})] = [A_0] + [A_1]\frac{\bar{s}}{U^*} + [A_2]\left(\frac{\bar{s}}{U^*}\right)^2 + \sum_{n=1}^{n_\beta}\left([A_{(n+2)}]\frac{\bar{s}}{\bar{s} + U^*\beta_n}\right) \tag{34}$$

where the β_n introduce the aerodynamic lags with respect to the structural modes. Moreover, n_β is the number of added poles and $[A_n]$ are the approximating coefficient matrices. The β_n and $[A_n]$ variables are determined by an optimized least-squares approximation method in which the nonlinear lag parameters are interactively evaluated with a simplex search method [27], whereas the linear coefficients are given by a simple least-squares fitting at each step [25]. Additionally, the number of added aerodynamic state variables is the same as the number of added poles, that is, $n_a = n_\beta$. For more details concerning this particular polynomial and its influence on the rest of the continuous-time formulation, please refer to [13,19].

For now, we are only interested in the remaining terms of the stability matrix of the resulting system, which are

$$[D_{\eta a}] = \begin{bmatrix} \frac{(U^*)^2}{\pi\mu}[\mathcal{M}]^{-1}[A_3] & \frac{(U^*)^2}{\pi\mu}[\mathcal{M}]^{-1}[A_4] & \cdots & \frac{(U^*)^2}{\pi\mu}[\mathcal{M}]^{-1}[A_{(n_a+2)}] \\ [0_{2\times2}] & [0_{2\times2}] & \cdots & [0_{2\times2}] \end{bmatrix} \tag{35}$$

$$[D_{a\eta}] = \begin{bmatrix} [I_{2\times2}] & [0_{2\times2}] \\ [I_{2\times2}] & [0_{2\times2}] \\ \vdots & \vdots \\ [I_{2\times2}] & [0_{2\times2}] \end{bmatrix}_{(2n_a\times4)} \tag{36}$$

$$[D_{aa}] = \begin{bmatrix} -U^*\beta_1[I_{2\times2}] & [0_{2\times2}] & \cdots & [0_{2\times2}] \\ [0_{2\times2}] & -U^*\beta_2[I_{2\times2}] & \cdots & [0_{2\times2}] \\ \vdots & \vdots & \ddots & \vdots \\ [0_{2\times2}] & [0_{2\times2}] & \cdots & -U^*\beta_{n_\beta}[I_{2\times2}] \end{bmatrix} \tag{37}$$

Eversman and Tewari Polynomials

The polynomial originally proposed by Eversman and Tewari [25,26] is very similar to the Roger polynomial. In the Laplace domain, it is written as

$$[A(\bar{s})] = [A_0] + [A_1]\frac{\bar{s}}{U^*} + [A_2]\left(\frac{\bar{s}}{U^*}\right)^2 + \sum_{n=1}^{n_\beta}\left([A_{(n+2)}]\frac{U^*}{\bar{s} + U^*\beta_n}\right) \tag{38}$$

where, once again, the β_n introduce the aerodynamic lags with respect to the structural modes. Similarly, the variables of the polynomial are also determined by the same optimized least-squares approximation method as in the Roger polynomial case. Once again, the number of augmented states is equal to the number of added poles, that is, $n_a = n_\beta$.

In this case, the stability matrix is given by

$$[D_{\eta a}] = \begin{bmatrix} \frac{(U^*)^3}{\pi\mu}[\mathcal{M}]^{-1}[A_3] & \frac{(U^*)^3}{\pi\mu}[\mathcal{M}]^{-1}[A_4] & \cdots & \frac{(U^*)^3}{\pi\mu}[\mathcal{M}]^{-1}[A_{(n_a+2)}] \\ [0_{2\times2}] & [0_{2\times2}] & \cdots & [0_{2\times2}] \end{bmatrix} \tag{39}$$

$$[D_{a\eta}] = \begin{bmatrix} [0_{2\times2}] & [I_{2\times2}] \\ [0_{2\times2}] & [I_{2\times2}] \\ \vdots & \vdots \\ [0_{2\times2}] & [I_{2\times2}] \end{bmatrix}_{(2n_a\times4)} \tag{40}$$

whereas the $[D_{aa}]$ term is exactly the same one given by Eq. (37).

Eversman and Tewari [26] suggest that this model of aerodynamic state variables provides a better representation of the aerodynamic delays than the one suggested by Roger [13]. Furthermore, Eversman and Tewari [25] identified a repeated pole problem that may occur with both formulations. This problem consists of the occurrence of poles very close to each other. Whenever this happens, the linear $[A_n]$ coefficients corresponding to these lag parameters are very close in magnitude, very large, and of opposite signs. Such a phenomenon makes the subsequent eigenvalue problem poorly conditioned. To overcome such difficulty, Eversman and Tewari [25] suggest a slight modification to the lag terms in such situations.

When two poles are very close to each other, Eversman and Tewari [25] show that these poles can be represented by only one of them. However, this pole must appear in two terms of the polynomial, one linear and one quadratic. Moreover, the same type of analysis can be extended in the case of three, four, or actually any number of poles that occur very close to each other in the original formulation. With this approach, and for a given unsteady aerodynamic data set, the number of aerodynamic state variables added to the model remains the same, whereas the number of poles is reduced. Eversman and Tewari [25] demonstrate that this procedure does not alter the fitting accuracy of a given polynomial, but it results in a better conditioned eigenvalue problem. Therefore, in many cases, the following approximating polynomial is a more useful model than the original one given in Eq. (38):

$$\begin{aligned}[A(\bar{s})] = {} & [A_0] + [A_1]\frac{\bar{s}}{U^*} + [A_2]\left(\frac{\bar{s}}{U^*}\right)^2 \\ & + \sum_{n=1}^{n_\beta}\left([A_{(n+2)}]\frac{U^*}{\bar{s} + U^*\beta_n}\right) \\ & + \sum_{n=(n_{\beta_1}+1)}^{n_\beta}\left([A_{(n+N_2+2)}]\frac{U^{*2}}{(\bar{s} + U^*\beta_n)^2}\right) \\ & + \sum_{n=(n_{\beta_2}+1)}^{n_\beta}\left([A_{(n+N_3+2)}]\frac{U^{*3}}{(\bar{s} + U^*\beta_n)^3}\right) \\ & + \sum_{n=(n_{\beta_3}+1)}^{n_\beta}\left([A_{(n+N_4+2)}]\frac{U^{*4}}{(\bar{s} + U^*\beta_n)^4}\right) + \cdots \end{aligned} \tag{41}$$

with

$$\begin{gathered} N_2 = n_\beta - n_{\beta_1}, \qquad N_3 = 2n_\beta - n_{\beta_1} - n_{\beta_2} \\ N_4 = 3n_\beta - n_{\beta_1} - n_{\beta_2} - n_{\beta_3}, \cdots \end{gathered} \tag{42}$$

where n_β is the total number of poles and it is assumed that $\beta_1, \ldots, \beta_{n_{\beta_1}}$ are nonrepeated poles, $\beta_{(n_{\beta_1}+1)}, \ldots, \beta_{n_{\beta_2}}$ are poles that occur twice, $\beta_{(n_{\beta_2}+1)}, \ldots, \beta_{n_{\beta_3}}$ are poles that occur three times, and so on.

Notice that, in this case, the number of aerodynamic states is

$$n_a = n_\beta + (n_\beta - n_{\beta_1}) + (n_\beta - n_{\beta_2}) + \cdots \tag{43}$$

Furthermore, Eversman and Tewari [25] also argue that this alternate formulation may significantly reduce the computational time required for the optimization procedure, because the total number of poles is decreased for the same number of aerodynamic states.

In the present case, the stability matrix of the aeroelastic problem is composed of

$$[D_{\eta a}] = \begin{bmatrix} \frac{(U^*)^3}{\pi\mu}[\mathcal{M}]^{-1}[\tilde{A}_1] & \frac{(U^*)^4}{\pi\mu}[\mathcal{M}]^{-1}[\tilde{A}_2] & \frac{(U^*)^5}{\pi\mu}[\mathcal{M}]^{-1}[\tilde{A}_3] & \cdots \\ [0_{2\times 2n_\beta}] & [0_{2\times 2(n_\beta - n_{\beta_1})}] & [0_{2\times 2(n_\beta - n_{\beta_2})}] & \cdots \end{bmatrix} \tag{44}$$

$$[D_{a\eta}] = \begin{bmatrix} [0_{2n_\beta \times 2}] & [\tilde{I}] \\ [0_{2(n_a - n_\beta)\times 2}] & [0_{2(n_a - n_\beta)\times 2}] \end{bmatrix} \tag{45}$$

$$[D_{aa}] = \begin{bmatrix} [R_1] & [0_{2n_\beta \times 2(n_\beta - n_{\beta_1})}] & [0_{2n_\beta \times 2(n_\beta - n_{\beta_2})}] & \cdots \\ [0_{2(n_\beta - n_{\beta_1})\times 2n_\beta}] & [R_2] & [0_{2(n_\beta - n_{\beta_1})\times 2(n_\beta - n_{\beta_2})}] & \cdots \\ [0_{2(n_\beta - n_{\beta_2})\times 2n_\beta}] & [0_{2(n_\beta - n_{\beta_2})\times 2(n_\beta - n_{\beta_1})}] & [R_3] & \cdots \\ \vdots & \vdots & \vdots & \ddots \end{bmatrix} + \begin{bmatrix} [0_{2\times 2}] & [0_{2\times 2}] & [0_{2\times 2}] & \cdots \\ [I_{2\times 2}] & [0_{2\times 2}] & [0_{2\times 2}] & \cdots \\ [0_{2\times 2}] & [I_{2\times 2}] & [0_{2\times 2}] & \cdots \\ \vdots & \vdots & \ddots & \vdots \end{bmatrix} \tag{46}$$

where

$$[\tilde{A}_1] = [[A_3] \quad [A_4] \quad \cdots \quad [A_{(n_\beta+2)}]] \tag{47}$$

$$[\tilde{A}_2] = [[A_{(n_{\beta_1}+N2+3)}] \quad [A_{(n_{\beta_1}+N2+4)}] \cdots [A_{(n_\beta+N2)}]] \tag{48}$$

$$[\tilde{A}_3] = [[A_{(n_{\beta_2}+N3+3)}] \quad [A_{(n_{\beta_2}+N3+4)}] \cdots [A_{(n_\beta+N3)}]], \cdots \tag{49}$$

$$[\tilde{I}] = \begin{bmatrix} [I_{2\times 2}] \\ [I_{2\times 2}] \\ \vdots \\ [I_{2\times 2}] \end{bmatrix}_{(2n_\beta \times 2)} \tag{50}$$

and

$$[R_1] = -U^* \begin{bmatrix} \beta_1[I_{2\times 2}] & \cdots & [0_{2\times 2}] \\ \vdots & \ddots & \vdots \\ [0_{2\times 2}] & \cdots & \beta_{n_\beta}[I_{2\times 2}] \end{bmatrix} \tag{51}$$

$$[R_2] = -U^* \begin{bmatrix} \beta_{(n_{\beta_1}+1)}[I_{2\times 2}] & \cdots & [0_{2\times 2}] \\ \vdots & \ddots & \vdots \\ [0_{2\times 2}] & \cdots & \beta_{n_\beta}[I_{2\times 2}] \end{bmatrix} \tag{52}$$

$$[R_3] = -U^* \begin{bmatrix} \beta_{(n_{\beta_2}+1)}[I_{2\times 2}] & \cdots & [0_{2\times 2}] \\ \vdots & \ddots & \vdots \\ [0_{2\times 2}] & \cdots & \beta_{n_\beta}[I_{2\times 2}] \end{bmatrix}, \cdots \tag{53}$$

Noticing that, for a given number of augmented aerodynamic states, a multiple pole approximation is more efficient in the optimization process because of the reduction in lag parameters, Eversman and Tewari [25] extended this idea and suggested a third version for the approximating polynomial, which is given by

$$[A(\bar{s})] = [A_0] + [A_1]\bar{s} + [A_2]\bar{s}^2 + \sum_{n=1}^{n_a}\left([A_{(n+2)}]\frac{1}{(\bar{s}+\beta)^n}\right) \tag{54}$$

Therefore, in this case, there is only one lag parameter β, which occurs with multiplicity n_a. In this case, the stability matrix components are

$$[D_{\eta a}] = \begin{bmatrix} \frac{(U^*)^3}{\pi\mu}[\mathcal{M}]^{-1}[A_3] & \frac{(U^*)^4}{\pi\mu}[\mathcal{M}]^{-1}[A_4] & \cdots & \frac{(U^*)^{(n_a+2)}}{\pi\mu}[\mathcal{M}]^{-1}[A_{(n_a+2)}] \\ [0_{2\times 2}] & [0_{2\times 2}] & \cdots & [0_{2\times 2}] \end{bmatrix} \tag{55}$$

$$[D_{a\eta}] = \begin{bmatrix} [I_{2\times 2}] & [0_{2\times 2}] \\ [0_{2\times 2}] & [I_{2\times 2}] \\ [0_{2\times 2}] & [0_{2\times 2}] \\ \vdots & \vdots \\ [0_{2\times 2}] & [0_{2\times 2}] \end{bmatrix}_{(2n_a\times 4)} \tag{56}$$

$$[D_{aa}] = -U^*\beta[I_{2n_a\times 2n_a}] + \begin{bmatrix} [0_{2\times 2(n_a-1)}] & [0_{2\times 2}] \\ [I_{2(n_a-1)\times 2(n_a-1)}] & [0_{2(n_a-1)\times 2}] \end{bmatrix} \tag{57}$$

For more details concerning the Eversman and Tewari polynomials and their influence in the rest of the continuous-time formulation, please refer to [19,25,26].

In the present work, all four approximating models discussed are employed in a specific test case to address which one is more suitable for the complete aeroelastic analysis. This evaluation involves the compromise between fitting accuracy and conditioning of the eigenvalue problem.

Discrete-Time State-Space Formulation

Instead of approximating the discrete-time aerodynamic responses to make them suitable for application in Eq. (24), as presented in the previous section, another alternative is to represent every other time-dependent variable in a sampled, or discrete, manner. By doing so, it is possible to convert continuous-time state-space equations into discrete-time state-space equations and use digital control theory for the stability analysis [23]. The time step required for an accurate solution of the aerodynamic behavior must be small compared with the significant time constants of the system, which guarantees that no considerable error is introduced by the discretization procedure.

As indicated in [23], the solution of a continuous-time state-space system, such as the one represented in Eq. (21), is given by

$$\{x((n+1)\Delta\bar{t})\} = e^{([W]\Delta\bar{t})}\{x(n\Delta\bar{t})\} + e^{([W](n+1)\Delta\bar{t})}\int_{n\Delta\bar{t}}^{(n+1)\Delta\bar{t}} e^{(-[W]\tau)}\{q_x(\tau)\}\,\mathrm{d}\tau \tag{58}$$

where

$$[W] = -[\tilde{M}]^{-1}[\tilde{K}], \qquad \{q_x(\bar{t})\} = [\tilde{M}]^{-1}\{\tilde{q}(\bar{t})\} \tag{59}$$

It is very important to emphasize that the nondimensionalization of the aeroelastic system time step, $\Delta\bar{t}$, is not necessarily the same used for the time step of the flow solver. For example, according to the nondimensionalization of the flow variables generally used in CFD solvers, the correspondence between the aeroelastic and the aerodynamic time steps is given by

$$\Delta\hat{t} = (\Delta t)\frac{a_\infty}{2b}, \qquad \Delta\bar{t} = (\Delta t)\omega_r = \frac{U_\infty 2b}{a_\infty b}\frac{\Delta\hat{t}}{U^*} = \frac{2M_\infty}{U^*}\Delta\hat{t} \tag{60}$$

where $\Delta\hat{t}$ designates the flow solver time step. Considering that both time steps are small enough, it is reasonable to assume

$$\{\bar{Q}a(\bar{t})\} = \{\bar{Q}a(n\Delta\bar{t})\}, \qquad n\Delta\bar{t} \le \bar{t} < (n+1)\Delta\bar{t} \tag{61}$$

and, consequently,

$$\{\tilde{q}(\bar{t})\} = \{\tilde{q}(n\Delta\bar{t})\}, \qquad n\Delta\bar{t} \le \bar{t} < (n+1)\Delta\bar{t} \tag{62}$$

$$\{q_x(\bar{t})\} = \{q_x(n\Delta\bar{t})\}, \qquad n\Delta\bar{t} \le \bar{t} < (n+1)\Delta\bar{t} \tag{63}$$

Hence, as demonstrated in [23], Eq. (58) can be rewritten as

$$\{x((n+1)\Delta\bar{t})\} = [G(\Delta\bar{t})]\{x(n\Delta\bar{t})\} + [H(\Delta\bar{t})]\{q_x(n\Delta\bar{t})\} \tag{64}$$

where

$$[G(\Delta\bar{t})] = e^{([W]\Delta\bar{t})} \tag{65}$$

$$[H(\Delta\bar{t})] = \int_0^{\Delta\bar{t}} e^{([W]\tau)}\,\mathrm{d}\tau = [W]^{-1}[e^{([W]\Delta\bar{t})} - [I_{4\times4}]] \tag{66}$$

Moreover, the sampling of the state and load vectors, $\{x(\bar{t})\}$ and $\{q_x(\bar{t})\}$, results in the following sequences, respectively:

$$\{x[n]\} = \{x((n-1)\Delta\bar{t})\} \tag{67}$$

$$\{q_x[n]\} = \{q_x((n-1)\Delta\bar{t})\} \tag{68}$$

Therefore, the discrete version of Eq. (64) is

$$\{x[n+1]\} = [G(\Delta\bar{t})]\{x[n]\} + [H(\Delta\bar{t})]\{q_x[n]\} \tag{69}$$

The z transform is an operation defined in the discrete-time context that is very similar to the Laplace transform in the continuous-time context [23]. Therefore, instead of using approximating polynomials for the discrete aerodynamic response, it may be more convenient to perform the frequency domain analysis with the application of the z transform, or z domain analysis. The present formulation is based on the one-sided z transform, defined as

$$Y(z) = \mathcal{Z}\{y[n]\} = \sum_{n=0}^{\infty} y[n]z^{-n} \tag{70}$$

where $Y(z)$ is the z transform of the discrete sequence $y[n]$. Ogata [23] shows that, for an equivalent sampled function, that is,

$$y(t) = \begin{cases} y[n+1], & t = n\Delta t, \\ 0, & \text{otherwise} \end{cases} \tag{71}$$

the Laplace transform, $Y(s)$, is formally the same as the z transform, $Y(z)$, for the values of s that respect

$$s = (1/\Delta t)\,\ell_n\, z \tag{72}$$

Furthermore, it is important to notice that the definition of the z transform itself results in a polynomial in the z domain. This fact facilitates the construction of the state-space model, avoiding the need for a polynomial fitting process.

One very important theorem concerning the z transform is the shifting theorem [23]. This theorem states that, if $y[n] = 0$ for $n < 0$, then

$$\mathcal{Z}\{y[n+j]\} = z^j Y(z) \tag{73}$$

Consequently, the z transform of Eq. (69) yields

$$z\{X(z)\} = [G(\Delta\bar{t})]\{X(z)\} + [H(\Delta\bar{t})]\{Q_x(z)\} \tag{74}$$

Thus, the formulation of the discrete aeroelastic problem depends on the determination of the forcing term, $\{Q_x(z)\}$ in the z domain. Moreover, Oppenheim and Schafer [21] show that the z transform also presents the convolution theorem property, which states that the z transform of the convolution sum of two sequences is identical to the multiplication of their individual z transforms, that is,

$$\mathcal{Z}\{y_1[n] * y_2[n]\} = \mathcal{Z}\left\{\sum_{j=-\infty}^{\infty} y_1[j]y_2[n-j]\right\} = Y_1(z)Y_2(z) \tag{75}$$

Therefore, the discrete-time, z-domain, equivalent statement of the hypothesis adopted in Eq. (14) is

$$\{\bar{Q}a(z)\} = ((U^*)^2/\pi\eta)[A(z)]\{\eta(z)\} \tag{76}$$

where

$$[A(z)] = \begin{bmatrix} -C_{\ell_{Ih}}(z)/2 & -C_{\ell_{I\alpha}}(z) \\ C_{m_{Ih}}(z) & 2C_{m_{I\alpha}}(z) \end{bmatrix} \tag{77}$$

Hence,

$$\{Q_x(z)\} = [\tilde{M}]^{-1}\begin{Bmatrix} \{\bar{Q}a(z)\} \\ \{0_{2\times1}\} \end{Bmatrix} = \frac{(U^*)^2}{\pi\mu}[\tilde{M}]^{-1}\begin{Bmatrix} [A(z)]\{\eta(z)\} \\ \{0_{2\times1}\} \end{Bmatrix} \tag{78}$$

As explained in [21], a direct consequence of the convolution property is that the sought z transforms of the aerodynamic coefficients, which constitute the terms of the aerodynamic influence coefficient matrix, are given in the following form:

$$\begin{aligned} C_{\ell_{Ih}}(z) &= \frac{C_{l_{h\text{out}}}(z)}{h_{\text{in}}(z)}, \qquad & C_{m_{Ih}}(z) &= \frac{C_{m_{h\text{out}}}(z)}{h_{\text{in}}(z)} \\ C_{\ell_{I\alpha}}(z) &= \frac{C_{l_{\alpha\text{out}}}(z)}{\alpha_{\text{in}}(z)}, \qquad & C_{m_{I\alpha}}(z) &= \frac{C_{m_{\alpha\text{out}}}(z)}{\alpha_{\text{in}}(z)} \end{aligned} \tag{79}$$

where $C_{\ell_{h\text{out}}}(z)$, $C_{m_{h\text{out}}}(z)$, $C_{\ell_{\alpha\text{out}}}(z)$, and $C_{m_{\alpha\text{out}}}(z)$ are the z transforms of the time histories of the aerodynamic responses in terms of the corresponding coefficients, whereas $h_{\text{in}}(z)$ and $\alpha_{\text{in}}(z)$ are the z transforms of the input excitations in the plunge and pitch modes, respectively. For the sake of simplicity, the development of the aerodynamic state variables is henceforth only demonstrated for C_{ℓ_h}, and the results are then generalized for the other terms of the aerodynamic coefficient matrix.

Therefore, according to the suggestions of [23], by defining the auxiliary function

$$Y_h(z) = \frac{\xi(z)}{a_h(z)} \tag{80}$$

where

$$a_h(z) = 1 + a_{h_1}z^{-1} + a_{h_2}z^{-2} + \cdots + a_{h_{(n_T-1)}}z^{-(n_T-1)} \tag{81}$$

$$a_{h_n} = \frac{h_{\text{in}}[n+1]}{h_{\text{in}}[1]} \tag{82}$$

and n_T is the total number of points that constitute the aerodynamic response sequence, it is possible to construct the following aerodynamic state variables:

$$\begin{aligned} Xa_{h_1}(z) &= z^{-(n_T-1)}Y_h(z) \\ Xa_{h_2}(z) &= z^{-(n_T-2)}Y_h(z) \\ &\vdots \\ Xa_{h_{(n_T-1)}}(z) &= z^{-1}Y_h(z) \end{aligned} \tag{83}$$

These new states relate to each other by

$$zXa_{h_1}(z) = Xa_{h_2}(z)$$
$$zXa_{h_2}(z) = Xa_{h_3}(z)$$
$$\vdots$$
$$zXa_{h_{(n_T-2)}}(z) = Xa_{h_{(n_T-1)}}(z) \tag{84}$$

and Eq. (80) results in

$$zXa_{h_{(n_T-1)}}(z) = -a_{h_1}Xa_{h_{(n_T-1)}}(z) - a_{h_2}Xa_{h_{(n_T-2)}}(z) - \ldots - a_{h_{(n_T-1)}}Xa_{h_1}(z) + \xi(z) \tag{85}$$

Hence, Eqs. (84) and (85) can be rewritten in matrix form, as follows:

$$z\{Xa_h(z)\} = \begin{bmatrix} 0 & 1 & 0 & \cdots & 0 \\ 0 & 0 & 1 & \cdots & 0 \\ \vdots & \vdots & \vdots & \ddots & \vdots \\ 0 & 0 & 0 & \cdots & 1 \\ -a_{h_{(n_T-1)}} & -a_{h_{(n_T-2)}} & -a_{h_{(n_T-3)}} & \cdots & -a_{h_1} \end{bmatrix} \{Xa_h(z)\} + [0 \quad 0 \quad \cdots \quad 0 \quad 1]^T \xi(z) \tag{86}$$

where the z transform of the aerodynamic state vector is given by

$$\{Xa_h(z)\} = \begin{Bmatrix} Xa_{h_1}(z) \\ Xa_{h_2}(z) \\ \vdots \\ Xa_{h_{(n_T-1)}}(z) \end{Bmatrix} \tag{87}$$

Furthermore, from Eq. (79), one can obtain

$$C_{\ell_{Ih}}(z) = \frac{C_{\ell_{h\text{out}}}(z)}{h_{\text{in}}(z)} = \frac{C_{\ell_{h\text{out}}}[1]z^{-1} + \ldots + C_{\ell_{h\text{out}}}[n_T]z^{-n_T}}{h_{\text{in}}[1]z^{-1} + \ldots + h_{\text{in}}[n_T]z^{-n_T}} = \frac{-2[b_{C\ell h_0} + b_{C\ell h_1}z^{-1} + \ldots + b_{C\ell h_{(n_T-1)}}z^{-(n_T-1)}]}{a_h(z)} \tag{88}$$

where

$$b_{C\ell h_n} = -\frac{C_{\ell_{h\text{out}}}[n+1]}{2h_{\text{in}}[1]} \tag{89}$$

Then, neglecting for now the term related to the pitch mode in Eq. (10), one can write that

$$C_{\ell_h}(z) = C_{\ell_{Ih}}(z)\frac{\xi(z)}{2} = -b_{C\ell h_0}\xi(z) - \frac{\xi(z)}{a_h(z)}[(b_{C\ell h_1} - a_{h_1}b_{C\ell h_0})z^{-1} + \cdots + (b_{C\ell h_{(n_T-1)}} - a_{h_{(n_T-1)}}b_{C\ell h_0})z^{-(n_T-1)}] \tag{90}$$

Therefore, the lift coefficient due to the plunge mode is given in the z domain by

$$C_{\ell_h}(z) = -[\,c_{C\ell h_{(n_T-1)}} \quad c_{C\ell h_{(n_T-2)}} \quad \cdots \quad c_{C\ell h_1}\,]\{Xa_h(z)\} - b_{C\ell h_0}\xi(z) \tag{91}$$

where

$$c_{C\ell h_n} = b_{C\ell h_n} - a_{h_n}b_{C\ell h_0} \tag{92}$$

From such a formulation, it is straightforward to deduce that the $C_{m_h}(z)$ depends on the same aerodynamic state vector $\{Xa_h(z)\}$. Furthermore, in an analogous way, it is possible to define similar concepts for the pitch mode. Therefore, it is possible to put all these definitions together to construct a general state-space representation for the generalized aerodynamic forces in the z domain. First of all, one can define

$$a_\alpha = 1 + a_{\alpha_1}z^{-1} + a_{\alpha_2}z^{-2} + \cdots + a_{\alpha_{n_T-1}}z^{-(n_T-1)} \tag{93}$$

$$a_{\alpha_n} = \frac{\alpha_{\text{in}}[n+1]}{\alpha_{\text{in}}[1]} \tag{94}$$

$$b_{C\ell\alpha_n} = -\frac{C_{\ell_{\alpha\text{out}}}[n+1]}{\alpha_{\text{in}}[1]} \tag{95}$$

$$b_{Cm\alpha_n} = \frac{2C_{m_{\alpha\text{out}}}[n+1]}{\alpha_{\text{in}}[1]} \tag{96}$$

$$b_{Cmh_n} = \frac{C_{m_{h\text{out}}}[n+1]}{h_{\text{in}}[1]} \tag{97}$$

and

$$\{Ya(z)\} = \begin{bmatrix} \frac{1}{a_h(z)} & 0 \\ 0 & \frac{1}{a_\alpha(z)} \end{bmatrix}\{\eta(z)\} \tag{98}$$

$$\{Xa_1(z)\} = z^{-(n_T-1)}\{Ya(z)\}$$
$$\{Xa_2(z)\} = z^{-(n_T-2)}\{Ya(z)\}$$
$$\vdots$$
$$\{Xa_{(n_T-1)}(z)\} = z^{-1}\{Ya(z)\} \tag{99}$$

These aerodynamic states relate to each other by

$$z\{Xa_1(z)\} = \{Xa_2(z)\}$$
$$z\{Xa_2(z)\} = \{Xa_3(z)\}$$
$$\vdots$$
$$z\{Xa_{(n_T-2)}(z)\} = \{Xa_{(n_T-1)}(z)\} \tag{100}$$

and

$$z\{Xa_{(n_T-1)}(z)\} = [\,-[\bar{A}_{(n_T-1)}] \quad -[\bar{A}_{(n_T-2)}] \quad \cdots \quad -[\bar{A}_1]\,]\{Xa(z)\} + [I_{2\times2}]\{\eta(z)\} \tag{101}$$

where the z transform of the aerodynamic state vector is given by

$$\{Xa(z)\} = \begin{Bmatrix} \{Xa_1(z)\} \\ \{Xa_2(z)\} \\ \vdots \\ \{Xa_{(n_T-1)}(z)\} \end{Bmatrix} \tag{102}$$

and

$$[\bar{A}_n] = \begin{bmatrix} a_{h_n} & 0 \\ 0 & a_{\alpha_n} \end{bmatrix} \tag{103}$$

Finally, it is possible to describe the forcing term, $\{Q_x(z)\}$, through the new state-space representation, as follows:

$$\{Q_x(z)\} = [Aa]\{Xa(z)\} + [Ax]\{X(z)\} \tag{104}$$

where

$$[Aa] = \frac{(U^*)^2}{\pi\mu}[\tilde{M}]^{-1}\begin{bmatrix} [B] \\ [0_{2\times(2n_T-2)}] \end{bmatrix} \tag{105}$$

$$[Ax] = \frac{(U^*)^2}{\pi\mu}[\tilde{M}]^{-1}\begin{bmatrix}[0_{2\times2}] & [B_0]\\ [0_{2\times2}] & [0_{2\times2}]\end{bmatrix} \tag{106}$$

$$[B] = \begin{bmatrix}[B_{C\ell_{(n_T-1)}}] & [B_{C\ell_{(n_T-2)}}] & \cdots & [B_{Cl_1}]\\ [B_{Cm_{(n_T-1)}}] & [B_{Cm_{(n_T-2)}}] & \cdots & [B_{Cm_1}]\end{bmatrix} \tag{107}$$

$$[B_{C\ell_n}] = [\, b_{C\ell h_n} - a_{h_n} b_{C\ell h_0} \quad b_{C\ell\alpha_n} - a_{\alpha_n} b_{C\ell\alpha_0}\,] \tag{108}$$

$$[B_{Cm_n}] = [\, b_{Cmh_n} - a_{h_n} b_{Cmh_0} \quad b_{Cm\alpha_n} - a_{\alpha_n} b_{Cm\alpha_0}\,] \tag{109}$$

and

$$[B_0] = \begin{bmatrix} b_{C\ell h_0} & b_{C\ell\alpha_0}\\ b_{Cmh_0} & b_{Cm\alpha_0}\end{bmatrix} \tag{110}$$

Hence, Eq. (104) describes a state-space representation in the z domain that is adequate for application in Eq. (74). The final expression for the state-space problem is then given by

$$([\bar{D}] - z[I_{N\times N}])\{\bar{\chi}(z)\} = \{0_{N\times1}\} \tag{111}$$

where

$$[\bar{D}] = \begin{bmatrix}[\bar{D}xx] & [\bar{D}xa]\\ [\bar{D}ax] & [\bar{D}aa]\end{bmatrix} \tag{112}$$

$$[\bar{D}xx] = [G(\Delta\bar{t})] + [H(\Delta\bar{t})][Ax] \tag{113}$$

$$[\bar{D}xa] = [H(\Delta\bar{t})][Aa] \tag{114}$$

$$[\bar{D}ax] = \begin{bmatrix}[0_{(2n_T-4)\times2}] & [0_{(2n_T-4)\times2}]\\ [0_{2\times2}] & [I_{2\times2}]\end{bmatrix} \tag{115}$$

and

$$[\bar{D}aa] = \begin{bmatrix}[0_{2\times2}] & [I_{2\times2}] & [0_{2\times2}] & \cdots & [0_{2\times2}]\\ [0_{2\times2}] & [0_{2\times2}] & [I_{2\times2}] & \cdots & [0_{2\times2}]\\ \vdots & \vdots & \vdots & \ddots & \vdots\\ [0_{2\times2}] & [0_{2\times2}] & [0_{2\times2}] & \cdots & [I_{2\times2}]\\ -[\bar{A}_{(n_T-1)}] & -[\bar{A}_{(n_T-2)}] & -[\bar{A}_{(n_T-3)}] & \cdots & -[\bar{A}_1]\end{bmatrix} \tag{116}$$

Here, N designates the total number of states, which is given by $N = (2n_T + 2)$. The state vector, $\{\bar{\chi}\}$, is formed by all the structural and aerodynamic state variables, and its z transform is defined as

$$\{\bar{\chi}(z)\} = \begin{Bmatrix}\{X(z)\}\\ \{Xa(z)\}\end{Bmatrix} \tag{117}$$

Although this discrete-time formulation does not require the construction of approximating polynomials, it has one drawback. The formulation indicates that the number of augmented aerodynamic state vectors is the same as the number of time steps needed to accurately represent the unsteady aerodynamic response. Therefore, the size of the eigenvalue problem is much larger than in the continuous-time formulation. The number of state variables may be hundreds or thousands of times larger in the discrete-time case. However, because in well-constructed root locus analyses the eigenvalues vary little from each other for two consecutive values of the root locus parameter, there are numerical schemes that can solve for the desired eigenvalues quite rapidly. The greatest limitation, then, is the memory size. In any event, this difficulty can be overcome by choosing an appropriate number of points to represent the aerodynamic response for a certain frequency range of interest. Moreover, because matrix $[\bar{D}]$ has very few nonzero elements, memory usage can be also reduced by employing techniques for construction of sparse matrices.

Direct Integration

A more straightforward manner of solving the aeroelastic problem is the simultaneous direct integration of the structural dynamic equations together with the flow unsteady equations. This may seem like a very natural procedure, but it turns out to be extremely costly as well. It is instructive, however, to compare the results given by the proposed state-space formulations with the direct integrations of the aeroelastic problem. For the two-dimensional Euler equations coupled with a simple typical section model, the computational cost, although much higher than for the state-space models, is not prohibitive. Therefore, a new version of the flow solver coupled with the structural dynamic equations is developed for validation purposes.

Before proceeding to the numerical discretization of the structural dynamic equations, it is very important to normalize these equations according to the nondimensionalization of the flow solver, such that both integrations advance at the same pace. The CFD code used in the present work [11,19] applies the time nondimensionalization indicated in the previous section. Thus, using the same nondimensionalization, Eq. (1) becomes

$$\ddot{\xi}(\hat{t}) + x_\alpha\ddot{\alpha}(\hat{t}) + \left(2\frac{M_\infty}{U^*}\frac{\omega_h}{\omega_r}\right)^2\xi(\hat{t}) = -\frac{4M_\infty^2}{\pi\mu}C\ell(\hat{t}) \tag{118}$$

$$x_\alpha\ddot{\xi}(\hat{t}) + r_\alpha^2\ddot{\alpha}(\hat{t}) + \left(2\frac{M_\infty r_\alpha}{U^*}\frac{\omega_\alpha}{\omega_r}\right)^2\alpha(\hat{t}) = \frac{8M_\infty^2}{\pi\mu}Cm(\hat{t}) \tag{119}$$

where M_∞ denotes the undisturbed flow Mach number.

The numerical integration of the structural dynamic equations is implemented following the suggestions in [28] with a very simple second-order accurate, centered difference scheme for the second derivative terms. Hence, the discretization yields

$$\ddot{\xi}((n+1)\Delta\hat{t}) \approx \frac{\xi[n+1] - 2\xi[n] + \xi[n-1]}{(\Delta\hat{t})^2}$$
$$\longrightarrow \xi[n+1] \approx (\Delta\hat{t})^2\ddot{\xi}((n+1)\Delta\hat{t}) + 2\xi[n] - \xi[n-1] \tag{120}$$

and, similarly,

$$\alpha[n+1] \approx (\Delta\hat{t})^2\ddot{\alpha}((n+1)\Delta\hat{t}) + 2\alpha[n] - \alpha[n-1] \tag{121}$$

The substitution of Eqs. (120) and (121) into Eqs. (118) and (119) yields, after some manipulation,

$$\xi[n+1] = \left[\frac{r_\alpha^2}{x_\alpha^2 - r_\alpha^2}\left(2\frac{M_\infty}{U^*}\frac{\omega_h}{\omega_r}\Delta\hat{t}\right)^2 + 2\right]\xi[n]$$
$$- \frac{x_\alpha r_\alpha^2}{x_\alpha^2 - r_\alpha^2}\left(2\frac{M_\infty}{U^*}\frac{\omega_\alpha}{\omega_r}\Delta\hat{t}\right)^2\alpha[n]$$
$$+ \frac{4(M_\infty\Delta\hat{t})^2}{\pi\mu(x_\alpha^2 - r_\alpha^2)}(r_\alpha^2 C_\ell[n] + 2x_\alpha C_m[n]) - \xi[n-1] \tag{122}$$

and

$$\alpha[n+1] = \left[\frac{r_\alpha^2}{x_\alpha^2 - r_\alpha^2}\left(2\frac{M_\infty}{U^*}\frac{\omega_\alpha}{\omega_r}\Delta\hat{t}\right)^2 + 2\right]\alpha[n]$$
$$- \frac{x_\alpha}{x_\alpha^2 - r_\alpha^2}\left(2\frac{M_\infty}{U^*}\frac{\omega_h}{\omega_r}\Delta\hat{t}\right)^2\xi[n] - \frac{4(M_\infty\Delta\hat{t})^2}{\pi\mu(x_\alpha^2 - r_\alpha^2)}(x_\alpha C_\ell[n]$$
$$+ 2C_m[n]) - \alpha[n-1] \tag{123}$$

Therefore, after having determined the values of C_ℓ and C_m at a given time step, the code uses Eqs. (122) and (123) for evaluating the new position of the airfoil. Then it returns to the flow solver algorithm, and this interactive process goes on until enough information is gathered to obtain the damping and frequency characteristics of the response. It is relevant to emphasize that one simulation is required for each value of the characteristic speed parameter, U^*. Thus, this approach requires as many simulations as necessary to bracket the flutter condition, with converging and diverging situations, until the desired accuracy is obtained.

Results and Discussion

The test case used in the present work considers the aeroelastic stability of a NACA 0012 airfoil at $M_\infty = 0.80$ and a zero initial angle of attack. The structural parameters that define the problem are $a_h = -2.0,\ x_\alpha = 1.8,\ r_\alpha = 1.865,\ \mu = 60,\ \omega_\alpha = 100$ rad/s, and $\omega_h = 100$ rad/s, and $\omega_r = \omega_\alpha$ is used as reference. This case is also reported in [8], in which the same sort of stability analysis is performed with aerodynamic data obtained through a numerical scheme very similar to the one used in the present work. It is important to note that the results shown in this paper are based on a pitching motion that occurs around the quarter-chord point of the airfoil, and that the moment coefficients are given with respect to that point. Because the elastic axis is located at another point, before proceeding to the aeroelastic stability analyses, the following transformations are necessary [2,29]:

$$\tilde{C}_{m_\alpha} = C_{m_\alpha} + rC_{\ell_\alpha} - rC_{m_h} - r^2 C_{\ell_h} \tag{124}$$

$$\tilde{C}_{m_h} = C_{m_h} + rC_{\ell_h} \tag{125}$$

$$\tilde{C}_{\ell_h} = C_{\ell_h} \tag{126}$$

$$\tilde{C}_{\ell_\alpha} = C_{\ell_\alpha} - rC_{\ell_h} \tag{127}$$

where

$$r = (a_h/2) - 0.25 \tag{128}$$

and the ($\sim$) variables denote the adapted coefficients.

The impulsive aerodynamic responses of both modes, in terms of the generalized force coefficients written in the frequency domain, are presented in Figs. 2 and 3 for the plunge and pitch modes, respectively. The results in Figs. 2 and 3 present the frequency content of the response up to $\kappa = 3.00$, because this is about the highest reduced frequency involved in the cases considered for the construction of the root locus stability analyses subsequently shown. The results obtained by the authors are those represented by the exponentially-shaped pulse (EP), because this is the type of excitation imposed to the aerodynamic system [20]. It is relevant to clarify that the actual EP responses obtained with the CFD code are not the impulsive aerodynamic responses shown in Figs. 2 and 3. These impulsive aerodynamic responses are obtained after some manipulations of the EP responses, as described in [20].

Figures 2 and 3 also include the aerodynamic responses to harmonic (H) motions at different reduced frequencies in both modes. Such responses are shown to address the linearity question brought up in a previous section of this paper. Oppenheim and Schafer [21] showed that obtaining impulsive responses from smooth excitations is only possible if the linearity assumptions, which are made in this work, hold. Therefore, the agreement between EP and H data is proof that such hypotheses are valid for small amplitudes. Furthermore, although Rausch et al. [8] offer comparison data only to reduced frequencies up to $\kappa = 1.00$, the present results match the literature (Lit.) values very closely in that range. This agreement is another assessment of the correctness of the present results. Further validation of the numerical tool used here can be found in [19,20].

The four interpolating polynomials discussed in the paper are applied to conveniently approximate the aerodynamic results. The authors use 1, 2, 3, 4, 6, and 10 augmented state variables in every case, except for the second form of the Eversman and Tewari (E and T-2) polynomial, which requires the occurrence of very close poles. Such a situation only happened in the case of four added states, when a double pole was observed. The fitting errors for all approximating models are presented in Fig. 4a. Here, the fitting error measure corresponds to the mean quadratic relative error, considering the four aerodynamic coefficients in the average, that is,

$$\mathrm{FE} = \frac{1}{4n_K}\left\{\sum_{i=1}^{n_K}\left[\left|\frac{(C_{\ell_h}(\kappa_i) - C^*_{\ell_h}(\kappa_i))^2}{R^2_{\ell_{hi}}}\right| + \left|\frac{(C_{m_h}(\kappa_i) - C^*_{m_h}(\kappa_i))^2}{R^2_{m_{hi}}}\right| + \left|\frac{(C_{\ell_\alpha}(\kappa_i) - C^*_{\ell_\alpha}(\kappa_i))^2}{R^2_{\ell_{\alpha i}}}\right| + \left|\frac{(C_{m_\alpha}(\kappa_i) - C^*_{m_\alpha}(\kappa_i))^2}{R^2_{m_{\alpha i}}}\right|\right]\right\} \tag{129}$$

where

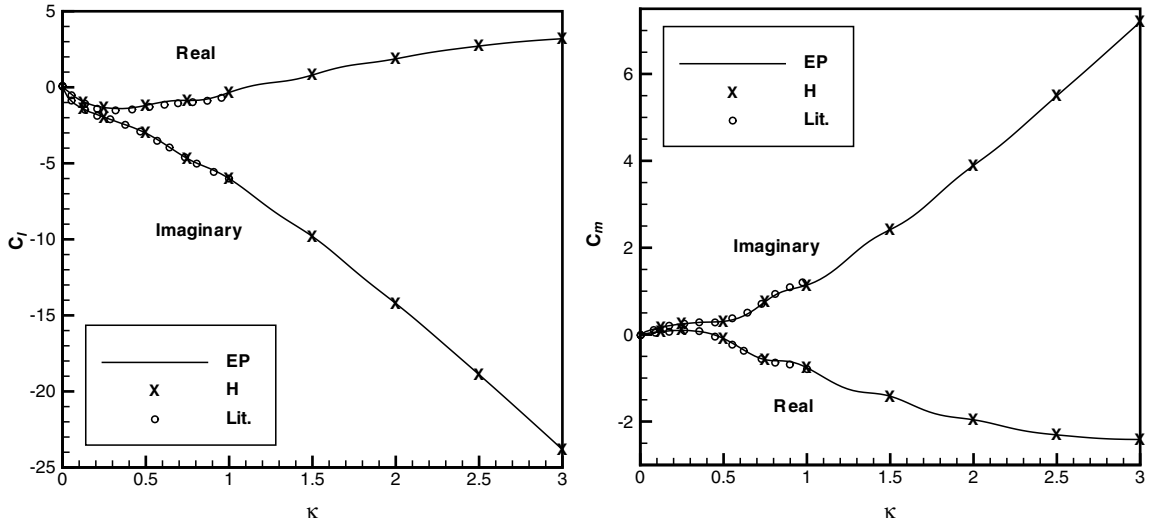

a) C_l frequency domain response b) C_m frequency domain response

Fig. 2 Reduced frequency response of a NACA 0012 airfoil at $M_\infty = 0.80$ and $\alpha_0 = 0$ to an impulsive input in the plunge mode.

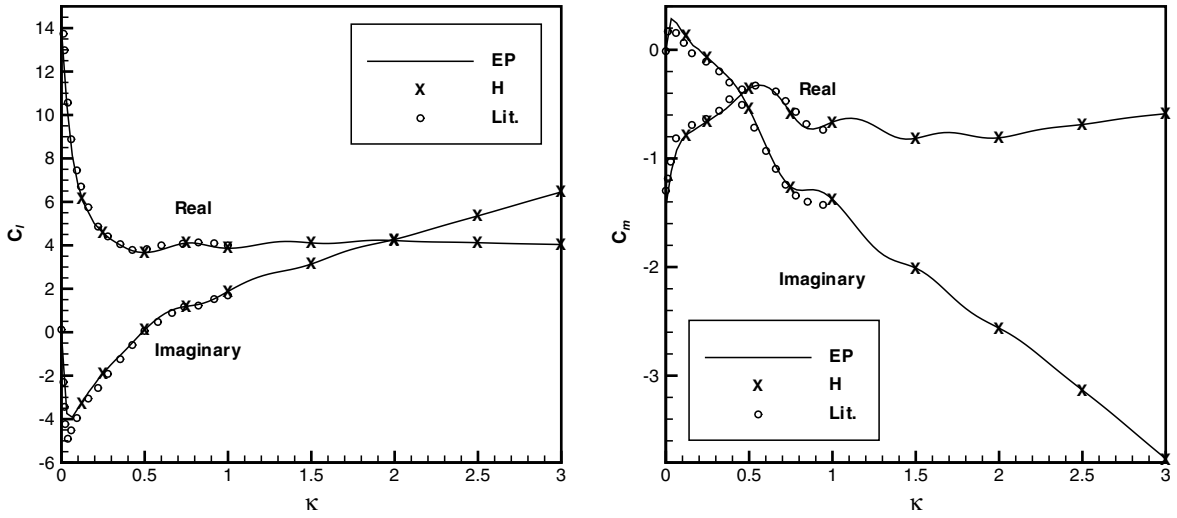

a) C_l frequency domain response b) C_m frequency domain response

Fig. 3 Reduced frequency response of a NACA 0012 airfoil at $M_\infty = 0.80$ and $\alpha_0 = 0$ to an impulsive input in the pitch mode.

$$R_{\ell_{h_i}} = \begin{cases} C_{\ell_h}(\kappa_i), & \text{if } C_{\ell_h}(\kappa_i) \neq 0, \\ 1.0, & \text{otherwise} \end{cases} \tag{130}$$

and $R_{m_{hi}}$, $R_{\ell_{\alpha i}}$, and $R_{m_{\alpha i}}$ are defined in a similar manner. Moreover, the $(*)$ coefficients are those given by the approximate model, and n_K is the number of samples used to represent the frequency range of interest. Opposite to what Eversman and Tewari [26] state, in the present case, the first form of the Eversman and Tewari (E and T-1) polynomial does not necessarily result in a better fit than the Roger polynomial. Actually, there are situations in which the inverse happens. However, the overall errors resulting from both models are very similar. In the only case in which the second form of the Eversman and Tewari polynomial could be used, the error is the same as for the first form, as expected. Nevertheless, the third form of the Eversman and Tewari (E and T-3) polynomial resulted in higher errors regardless of the number of augmented states. This result is probably a consequence of the smaller flexibility in the pole positioning. However, this last formulation indeed showed a much more rapid convergence of the optimization procedure, which is the main justification for its use.

It can be argued, however, that the computational cost of the optimization procedure is not significant, at least for current-day computers. Hence, it does not constitute a relevant parameter for the choice of the most adequate model. The really important influence in this selection is the effect of the polynomial model in the solution of the eigenvalue problem that defines the system stability. Figure 4b presents the error in the solution of the eigenvalue problem for a different number of augmented states. This error measure is based on the determinant of $([D] - \lambda[I_{N\times N}])$, scaled by the largest element of the $[D]$ matrix. Here, λ designates the eigenvalue corresponding to the pitch mode when $Q^* = 0.1$, which is the first point of the root locus to be presented in the forthcoming paragraphs. Q^* stands for the characteristic dynamic pressure, and it is directly related to U^* by

$$Q^* = (U^*)^2/\mu \tag{131}$$

Figure 4b indicates that, as the number of added state variables is increased, the eigenvalue problem becomes more difficult to solve due to ill-conditioning issues. Therefore, considering both aspects presented in Fig. 4, the authors chose the first form of the Eversman and Tewari polynomial with six poles for the remainder of the aeroelastic stability analyses reported here. Figures 5 and 6 show

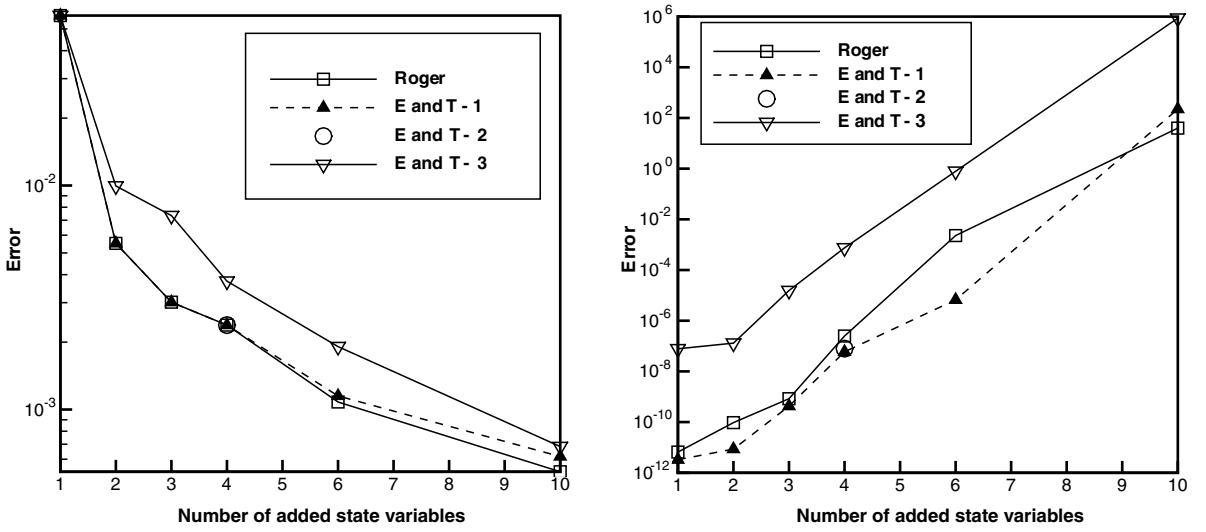

a) Fitting error for different interpolating polynomials b) Error in the solution of the first point of the eigenvalue problem

Fig. 4 Error parameters that influence the choice of the interpolating model.

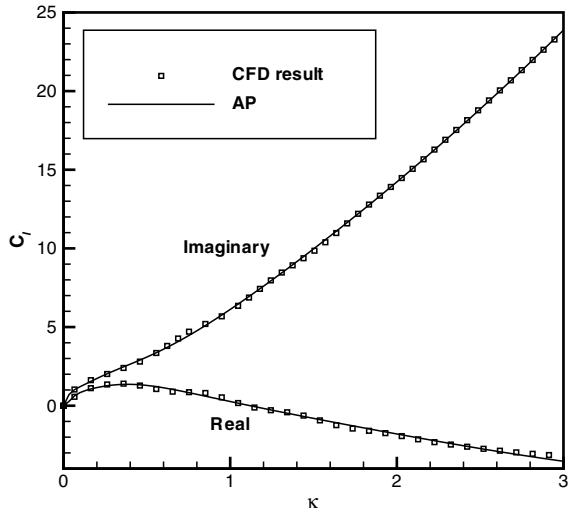

a) C_l frequency domain response

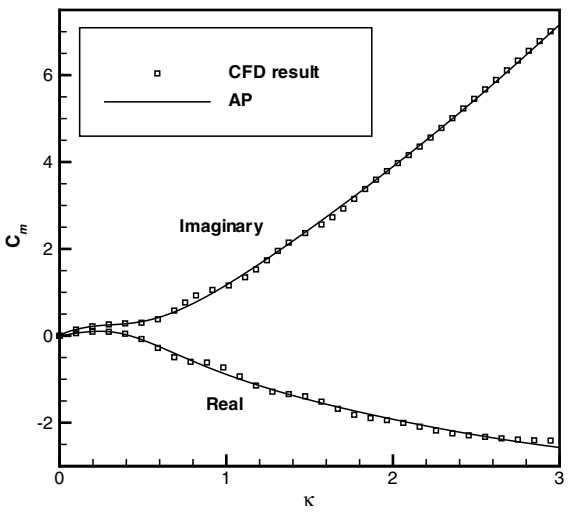

b) C_m frequency domain response

Fig. 5 Reduced frequency response of a NACA 0012 airfoil at $M_\infty = 0.80$ and $\alpha_0 = 0$ to an impulsive input in the plunge mode. Comparisons between CFD results and approximated data.

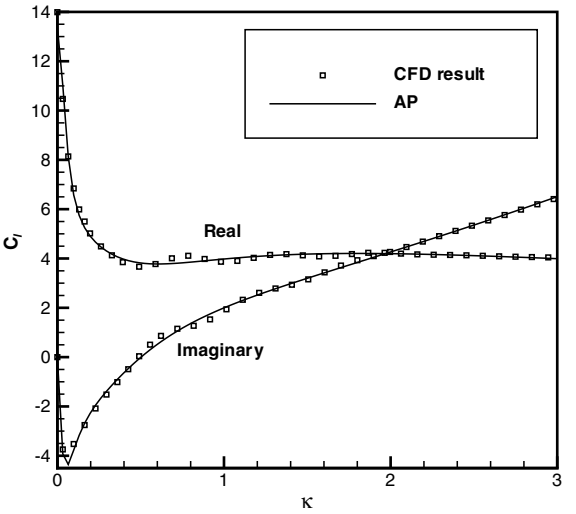

a) C_l frequency domain response

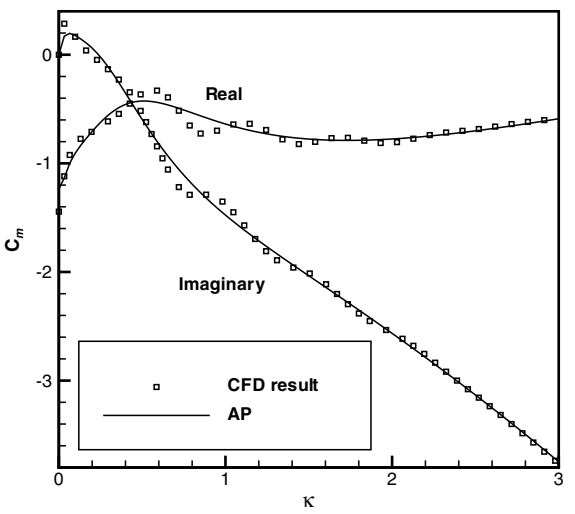

b) C_m frequency domain response

Fig. 6 Reduced frequency response of a NACA 0012 airfoil at $M_\infty = 0.80$ and $\alpha_0 = 0$ to an impulsive input in the pitch mode. Comparisons between CFD results and approximated data.

comparisons between the discrete CFD results and the chosen approximating (AP) model for the aerodynamic coefficients. The agreement between these data is extremely good, except for some small regions in which abrupt oscillations of the CFD results are smoothed by the polynomial. However, even in these regions, the fitting error is relatively small.

Finally, the stability analysis is concluded with the construction of a root locus graph, defined by the solution of the eigenvalue problem given by Eq. (33) for a continuous-time formulation or Eq. (111) for a discrete-time formulation. It is relevant to note that, in the discrete-time case, the eigenvalue problem is written in terms of the z variable, which is defined in a different manner than the s variable. However, they are related by Eq. (72). As the root locus is presented in terms of the nondimensional $\bar{s}$ variable, the real relationship used is

$$\bar{s} = \frac{s}{\omega_r} = \frac{1}{\Delta\bar{t}}\ell_n(z) = \frac{U^*}{2M_\infty \Delta\hat{t}}\ell_n(z) \tag{132}$$

Figures 7 and 8 present the root locus of the aeroelastic problem in question. The characteristic dynamic pressure parameter varies from $Q^* = 0.0$ up to 1.0 in $\Delta Q^* = 0.1$ intervals. Each plotted point corresponds to one of these values. The figures include the solutions

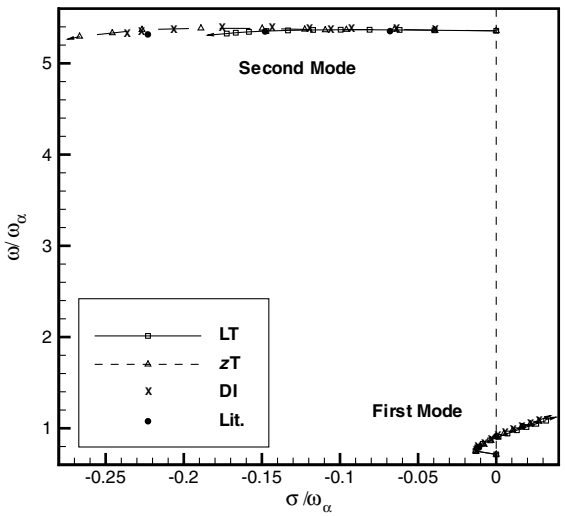

Fig. 7 Laplace domain root locus of the aeroelastic stability problem in question. Comparison of continuous-time, discrete-time, and direct integration calculations.

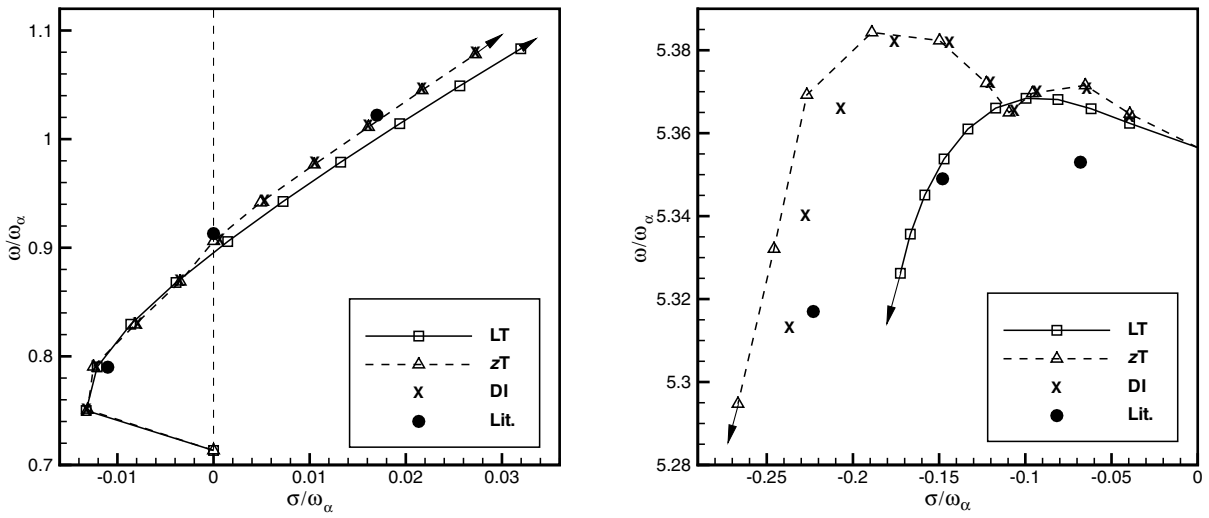

a) First aeroelastic mode curve

b) Second aeroelastic mode curve

Fig. 8 Individual view of each mode root locus.

obtained using the continuous-time Laplace transform (LT), the discrete-time z transform (zT), and the direct integration (DI) approaches, as well as the numerical direct integration results given in [8] (Lit.). The literature data, however, are only available for $Q^* = 0.2$, 0.5, and 0.8. Additionally, the results for the first two approaches are determined from the eigenvalue problems previously mentioned, whereas the damping and frequency characteristics of the direct integration responses are estimated using the modal identification technique of Bennet and Desmarais [30].

Before proceeding to further analyses, it is instructive to confirm that the employed aerodynamic responses are really sufficient for the correct solution of the present problem. For that, one should consider the higher reduced frequency content necessary for the construction of the root locus. The reduced frequency relates to the dimensionless frequency ω/ω_α by

$$\kappa = \frac{\omega b}{U_\infty} = \frac{1}{U^*}\frac{\omega}{\omega_\alpha} \tag{133}$$

Thus, the smaller the dynamic pressure, the higher the relevant reduced frequency range. Moreover, k is directly proportional to ω/ω_α, which indicates that the aeroelastic mode with the highest natural frequency determines the maximum range of reduced frequency in which the aerodynamic response must be known. In the present case, the second aeroelastic mode presents the highest natural frequency, $\omega/\omega_\alpha \approx 5.3$, and the minimum value of U^* considered is

$$U^*_{\min} = \sqrt{Q^*_{\min}\mu} = \sqrt{0.1 \times 60} \approx 2.45 \tag{134}$$

Then, $\kappa_{\max} \approx 2.16$. As the aerodynamic response is known for reduced frequency values up to 3.00, it represents the needed aerodynamic information for the stability analysis in question.

Furthermore, it is evident that the first aeroelastic mode curves and points obtained with the different methodologies agree much better than those in the second aeroelastic mode. The authors believe that this occurs for two main reasons. First of all, the modal identification technique used in the evaluation of the damping and frequency characteristics of the direct integration data (DI and lit.) is based on a curve fitting procedure applied simultaneously for both aeroelastic modes. It turns out that the time domain response of the most damped aeroelastic mode dies out much more rapidly than the response of the least damped aeroelastic mode. Hence, the least damped mode, which in the present case is the first aeroelastic mode, is favored in the curve fitting. The authors attempted to reduce this effect by using different sets of direct integration solutions for the determination of the frequency and damping characteristics of each aeroelastic mode. According to this approach, the most damped aeroelastic mode characteristics are evaluated with the initial portion of the direct integration solution, whereas the least damped aeroelastic mode characteristics are calculated using the whole solution. This procedure attenuates the damping difference effect, but it does not eliminate it. Moreover, the polynomial approximation for the aerodynamic coefficients produces the largest errors in the pitch mode responses for reduced frequency values between $\kappa = 0.5$ and 1.0 (see Figs. 5 and 6). According to Eq. (133), this means that these errors affect the continuous-time (LT) pitch mode root locus estimates mainly in the range of $0.5 \leq Q^* \leq 1.8$. As the plunge mode natural frequency is smaller, the influence of such errors on this mode is restricted to the range of $Q^* < 0.1$.

It is also important to note that the discrete-time (zT) root locus is the one that is closer to the DI results. This means that the z-domain state-space formulation suggested by the present authors is capable of adequately representing the aeroelastic system and provides an effective tool for determining flutter instability points. The larger errors observed in the continuous-time formulation are probably caused by inaccuracies that are intrinsic to the polynomial interpolation procedure. Moreover, the solution of the large eigenvalue problem given by the z-transform formulation has shown to be more practical, efficient, and accurate than using the continuous-time approach with its requirement for data approximation. Additionally, the authors' experience has shown that the large size of the aeroelastic stability matrix in the discrete-time case does not lead to ill-conditioning problems. Finally, as shown in Figs. 7 and 8, the literature data corroborate the quality of the results presented in the present paper. Even in the second aeroelastic mode case, in which the discrepancies are the largest, the relative differences are smaller than 1%, although the provided axis scales may seem to indicate otherwise.

At last, the flutter condition can be identified as the point at which one of the curves crosses the imaginary axis. A point-to-point linear interpolation of the results presented in Figs. 7 and 8 indicates the flutter frequency. Furthermore, Fig. 9 shows the damping behavior of the first aeroelastic mode in relation to the characteristic dynamic pressure and characteristic speed. The same sort of interpolation of such results yields the flutter characteristic dynamic pressure and characteristic speed. The flutter points acquired with the different approaches are shown in Table 1, in which the flutter prediction in [8] is also included. Actually, the literature value is given by a quadratic interpolation using the offered points. As can be seen, despite the mentioned discrepancies, the flutter predictions given by all methods are very similar, and the differences are not greater than 3% in any of the considered parameters.

Another way to construct a root locus based on the discrete-time results (zT) is in terms of the real and imaginary parts of the

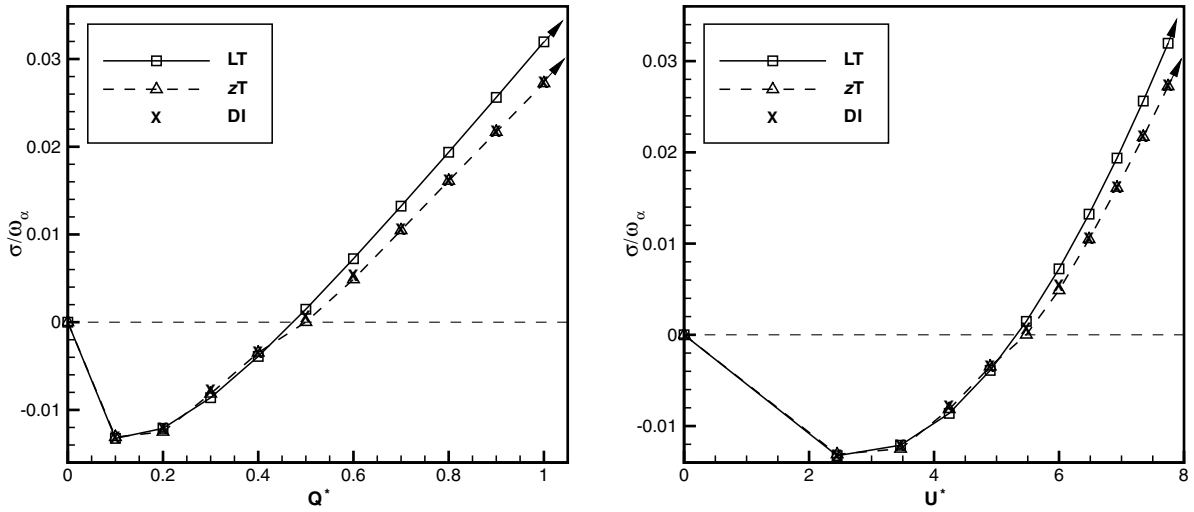

a) Characteristic dynamic pressure influence b) Characteristic speed influence

Fig. 9 First aeroelastic mode damping variation with respect to the characteristic dynamic pressure and characteristic speed.

eigenvalues in the z domain. This is shown in Fig. 10. However, due to the different definition of the z variable, the stability analysis is slightly different. As explained in [23], in this case, the imaginary axis of the usual Laplace domain graph is mapped onto the unitary circle around the origin in the z domain, whereas the left side of the s domain is mapped inside this circle and the right side is represented outside. Therefore, as long as the eigenvalues remain inside the unitary circle in the z domain, the system is stable, and the instability condition is given by the point at which one of the eigenvalues crosses that circle. Naturally, the result of the stability analysis is the same no matter which root locus representation is used. Additionally, it is important to emphasize that the z-domain root locus representation is quite unusual because the constant time step is the one used in the CFD solver ($\Delta\hat{t}$), whereas the aeroelastic formulation time step ($\Delta\tilde{t}$) is different for each value of Q^*, or U^*. Therefore, each point in this root locus corresponds to a different time step. However, this has no effect on the stability analysis.

The aeroelastic analysis methodologies proposed by the authors have been tested for a wide range of subsonic and transonic situations and proved to provide adequate results for flutter prediction in all cases [19]. Finally, it is possible to analyze the effects of the Mach number variation on the flutter phenomenon for the aeroelastic system considered in the present work. These effects are demonstrated in terms of the characteristic flutter dynamic pressure in Fig. 11a, the characteristic flutter speed in Fig. 11b, and the flutter frequency in Fig. 12. For all cases, the initial angle of attack is $\alpha_0 = 0$ deg.

As one can observe, from $M_\infty = 0.75$ on, the flutter characteristic dynamic pressure and speed experience a steeper drop. This is a reflection of the strong aerodynamic lag introduced by the presence of shock waves in the transonic regime, which occurs in that Mach number range. This type of phenomenon is known as "transonic dip," and it is one of the greatest motivations to employ sophisticated aerodynamic models in transonic flutter predictions, because the use of linear theories may perilously neglect this behavior and overpredict the flutter speed. It is also interesting to note that the flutter frequency decays considerably with the increase of the Mach number. Nevertheless, within the scope and objectives of the present work, the most relevant aspect of such results is the good agreement between state-space solutions and direct integration simulations. This demonstrates that it is possible to effectively and accurately predict flutter onset points with the approximate models proposed in the present paper, which present large computational savings when compared with direct integration schemes.

Table 1 Flutter points

Method	Q_f^*	U_f^*	ω/ω_α
DI	0.48	5.38	0.90
LT	0.47	5.32	0.90
zT	0.50	5.47	0.91
Lit.	0.50	5.48	0.91

Conclusions

The authors present a complete description of different state-space formulations for the representation of aeroelastic systems, including a new discrete-time, z-domain model adequate for aerodynamic unsteady responses obtained with numerical methods. Initially, some of the most common approximate models for the aerodynamic impulsive responses in the frequency domain are tested and compared. These approximate models supply the continuous-time state-space formulations with the required unsteady aerodynamic information necessary for the construction of root locus stability analyses. This procedure is then compared with the discrete-time formulation results. Comparisons of these results, and the ones provided by the direct integration of the structural dynamic and aerodynamic equations, demonstrate that the small fitting errors introduced by the approximating polynomials lead to some inaccuracies in the final stability analysis. The discrete-time formulation avoids such errors with the direct application of the z

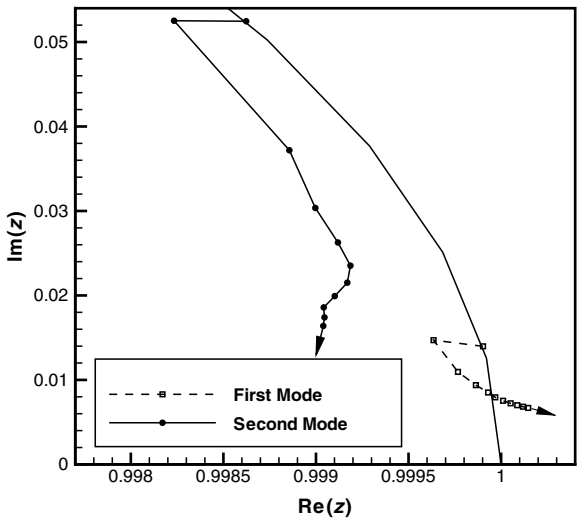

Fig. 10 z domain root locus of the aeroelastic stability problem in question.

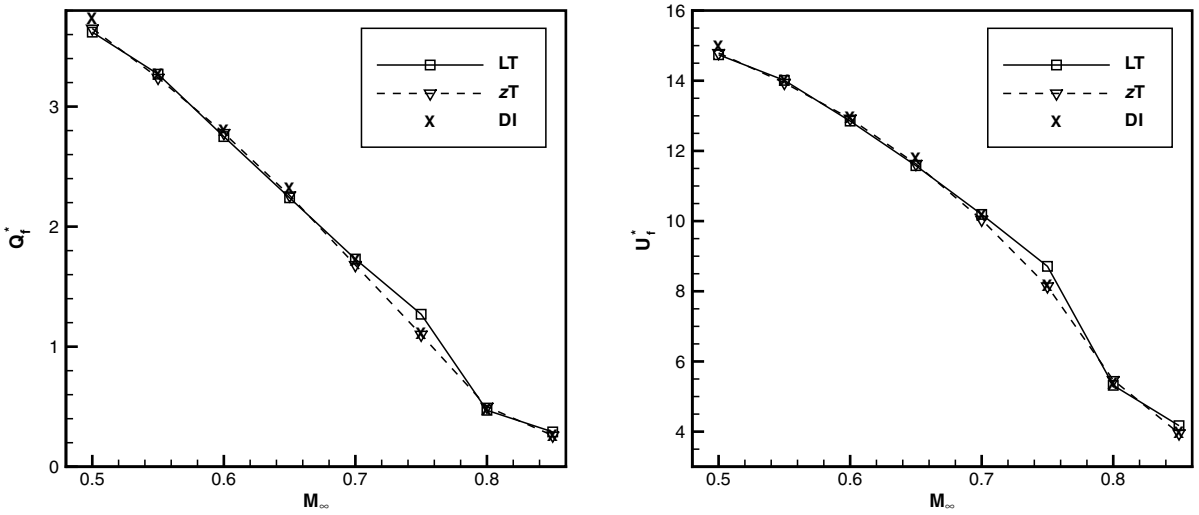

a) Flutter characteristic dynamic pressure b) Flutter characteristic speed

Fig. 11 Flutter characteristic dynamic pressure and characteristic speed variations with M_∞.

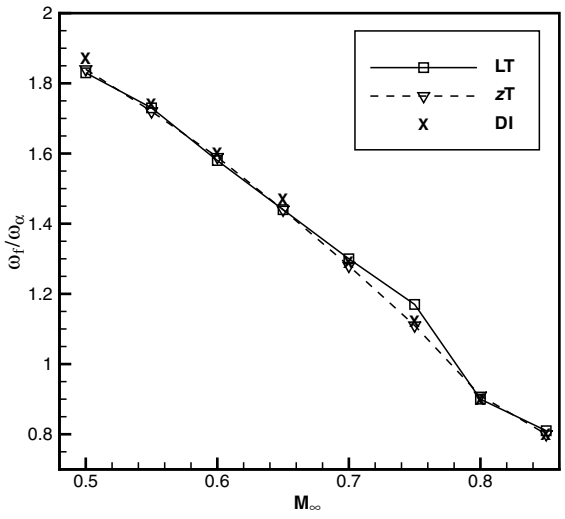

Fig. 12 Flutter frequency variation with M_∞.

transform to the time domain discrete aerodynamic data numerically obtained. Hence, this method has been shown to be more accurate than the previous state-space representations.

Furthermore, the approximate models used with the continuous-time formulations do not allow for a large number of aerodynamic state variables in the representation of the unsteady behavior, because this leads to ill-conditioning issues in the final eigenvalue problem. Therefore, although more accurate continuous representations of the aerodynamic responses are feasible through the addition of lag parameters, such an addition compromises the overall robustness of the aeroelastic results. On the other hand, the large number of aerodynamic state variables, which result from the z-domain state-space representation, do not affect the eigenvalue problem conditioning. Moreover, although this method leads to quite large stability matrices, only some of their terms present nonzero values. Thus, memory requirements can be lessened with the use of sparse matrix construction techniques.

Therefore, the paper shows that not only is a z-transform discrete-time state-space representation of aeroelastic systems possible, but it also is a very effective and accurate formulation. Furthermore, although optimization techniques facilitate the whole interpolating process, it still requires quite an annoying amount of work, especially if recurrent applications are considered. Because the representation of the aerodynamic response in the frequency domain can be evaluated with the application of the z transform, this new approach also seems to be a more straightforward method for standard parametric studies, which are typical of aeroelastic analyses. It is also important to emphasize that the discrete-time state-space formulation can also be very important in the field of aeroservoelasticity, because it allows for the determination of control laws suitable to digital control systems.

Finally, it is relevant to note that the aeroelastic analysis methodologies are successfully applied to typical section models involving subsonic and transonic flow configurations. The flutter points identified using the state-space formulations are generally very similar to each other and also similar to values predicted by the use of direct integration approaches. Hence, this demonstrates that the models proposed in the present work for efficient aeroelastic analyses are perfectly capable of offering good results even in the transonic regime.

Acknowledgments

The authors gratefully acknowledge the partial support for this research provided by Conselho Nacional de Desenvolvimento Científico e Tecnológico, CNPq, under the integrated project research grant no. 501200/2003-7 and 312064/2006-3. This work is also supported by Fundação de Amparo à Pesquisa do Estado de São Paulo, FAPESP, through an M.S. scholarship for the first author according to FAPESP process no. 04/11200-1. Further support from FAPESP is provided through process no. 04/16064-9.

References

[1] Dietze, F., "Air Forces of the Harmonically Vibrating Wing at Subsonic Velocity (Plane Problem)," Parts 1 and 2, U.S. Air Force Repts. F-TS-506-RE and F-TS-948-RE, 1947 (originally Luftfahrtforsch., Bd. 16, Lfg. 2, 1939, S. 84-96).

[2] Bisplinghoff, H. L., Ashley, H. L., and Halfman, R. L., *Aeroelasticity*, Adison–Wesley, Cambridge, MA, 1955.

[3] Fettis, H. E., "An Approximate Method for the Calculation of Nonstationary Air Forces at Subsonic Speeds," Wright Air Development Center, U.S. Air Force TR 52-56, 1952.

[4] Beam, R. M., and Warming, R. F., "Numerical Calculations of Two-Dimensional, Unsteady Transonic Flows with Circulation," NASA TN D-7605, Feb. 1974.

[5] Traci, R. M., Albano, E. D., and Farr, J. L., "Small Disturbance Transonic Flows About Oscillating Airfoils and Planar Wings," Air Force Flight Dynamics Laboratory TR-75-100, Aug. 1975.

[6] Ballhaus, W. F., and Goorjian, P. M., "Computation of Unsteady Transonic Flows by the Indicial Method," *AIAA Journal*, Vol. 16, No. 2, Feb. 1978, pp. 117–124. doi:10.2514/3.60868

[7] Batina, J. T., "Unsteady Euler Airfoil Solutions Using Unstructured Dynamic Meshes," AIAA Paper 89-0115, Jan. 1989.

[8] Rausch, R. D., Batina, J. T., and Yang, H. T. Y., "Euler Flutter Analysis

of Airfoils Using Unstructured Dynamic Meshes," *Journal of Aircraft*, Vol. 27, No. 5, May 1990, pp. 436–443. doi:10.2514/3.25295

[9] Oliveira, L. C., "A State-Space Aeroelastic Analysis Methodology Using Computational Aerodynamics Techniques," Master Thesis, Instituto Tecnológico de Aeronautica, São José dos Campos, São Paulo, Brazil, Aug. 1993 (in English).

[10] Raveh, D. E., "Reduced-Order Models for Nonlinear Unsteady Aerodynamics," *AIAA Journal*, Vol. 39, No. 8, Aug. 2001, pp. 1417–1429.

[11] Marques, A. N., and Azevedo, J. L. F., "Application of CFD-Based Unsteady Forces for Efficient Aeroelastic Stability Analyses," AIAA Paper No. 2006-0250, Jan. 2006.

[12] Vepa, R., "Finite State Modeling of Aeroelastic Systems," NASA CR-2779, Feb. 1977.

[13] Roger, K. L., "Airplane Math Modeling Methods for Active Control Design," AGARD CP-228, Aug. 1977.

[14] Abel, I., "An Analytical Technique for Predicting the Characteristics of a Flexible Wing Equipped with an Active Flutter-Suppression System and Comparison with Wind-Tunnel Data," NASA TP-1367, Hampton, VA, Feb. 1979.

[15] Dunn, H. J., "An Analytical Technique for Approximating Unsteady Aerodynamic in the Time Domain," NASA Langley Research Center TP-1738, Hampton, VA, Nov. 1980.

[16] Silva, W. A., and Raveh, D. E., "Development of Unsteady Aerodynamic State-Space Models from CFD-Based Pulse Responses," AIAA Paper No. 2001-1213, April 2001.

[17] Silva, W. A., and Bartels, R. E., "Development of Reduced-Order Models for Aeroelastic Analysis and Flutter Prediction Using the CFL3Dv6.0 Code," *Journal of Fluids and Structures*, Vol. 19, No. 6, July 2004, pp. 729–745. doi:10.1016/j.jfluidstructs.2004.03.004

[18] Kim, T., Hong, M., Bhatia, K. G., and Sengupta, G., "Aeroelastic Model Reduction for Affordable Computational Fluid Dynamics-Based Flutter Analysis," *AIAA Journal*, Vol. 43, No. 12, Dec. 2005, pp. 2487–2495. doi:10.2514/1.11246

[19] Marques, A. N., "A Unified Discrete-Time Approach for the State Space Representation of Aeroelastic Systems," M.S. Thesis, Instituto Tecnológico de Aeronautica, São José dos Campos, São Paulo, Brazil, Feb. 2007.

[20] Marques, A. N., and Azevedo, J. L. F., "A Survey on the Numerical Calculation of Impulsive and Indicial Aerodynamic Responses Using CFD Techniques," *25th AIAA Applied Aerodynamics Conference*, AIAA Paper 2007-4067, June 2007.

[21] Oppenheim, A. V., and Schafer, R. W., *Discrete-Time Signal Processing*, Prentice–Hall, Englewood Cliffs, NJ, 1989.

[22] Lin, J., and Iliff, K. W., "Aerodynamic Lift and Moment Calculations Using a Closed-Form Solution of the Possio Equation," NASA Dryden Flight Research Center TM-2000-209019, Edwards, CA, April 2000.

[23] Ogata, K., *Discrete-Time Control Systems*, Prentice–Hall, Englewood Cliffs, NY, 1987.

[24] Churchill, R. V., *Complex Variables and Applications*, 3rd ed., McGraw–Hill, New York, 1974.

[25] Eversman, W., and Tewari, A., "Consistent Rational-Function Approximation for Unsteady Aerodynamics," *Journal of Aircraft*, Vol. 28, No. 9, Sept. 1991, pp. 545–552. doi:10.2514/3.46062

[26] Eversman, W., and Tewari, A., "Modified Exponential Series Approximation for the Theodorsen Function," *Journal of Aircraft*, Vol. 28, No. 9, Sept. 1991, pp. 553–557. doi:10.2514/3.46063

[27] Lagarias, J. C., Reeds, J. A., Wright, M. H., and Wright, P. E., "Convergence Properties of the Nelder-Mead Simplex Method in Low Dimensions," *SIAM Journal on Optimization*, Vol. 9, No. 1, 1998, pp. 112–147. doi:10.1137/S1052623496303470

[28] Azevedo, J. L. F., "Transonic Aeroelastic Analysis of Launch Vehicle Configurations," NASA CR-4186, Oct. 1988.

[29] Yang, T. Y., Guruswamy, P., and Striz, A. G., "Flutter Analysis of a NACA 64A006 Airfoil in Small Disturbance Transonic Flow," *Journal of Aircraft*, Vol. 17, No. 4, April 1980, pp. 225–232. doi:10.2514/3.44652

[30] Bennet, R. M., and Desmarais, R. N., "Curve Fitting of Aeroelastic Transient Response Data with Exponential Functions," *Flutter Testing Techniques*, NASA Dryden Flight Research Center SP-415, Oct. 1975.